Global Simulations of Heat-Flux-Driven Buoyancy and Magnetothermal Instabilities, and their Astrophysical Implications

by

Ekapob Kulchoakrungsun

Submitted to the Department of Physics
in partial fulfillment of the requirements for the degree of

BACHELOR OF SCIENCE

at the

MASSACHUSETTS INSTITUTE OF TECHNOLOGY

June 2016

Signature of Author ..... Signature redacted
Department of Physics
May 20, 2016

Certified by..... Signature redacted .....
Professor Mark Vogelsberger
Assistant Professor
Thesis Supervisor

Accepted by ..... Signature redacted .....
Professor Nergis Mavalvala
Senior Thesis Coordinator, Department of Physics

Global Simulations of Heat-Flux-Driven Buoyancy and Magnetothermal Instabilities, and their Astrophysical Implications

by

Ekapob Kulchoakrungsun

Submitted to the Department of Physics
on May 20, 2016, in partial fulfillment of the
requirements for the degree of
BACHELOR OF SCIENCE

Abstract

In this thesis, we investigate the convective instabilities induced by anisotropic conduction in a rapidly conducting plasma. We simulate the magneto-thermal instability (MTI), and the heat-flux-driven buoyancy instability (HBI) in two- and three-dimensional, global hydrodynamic simulations performed by the AREPO code, and verify the results of previous works. Our results have important astrophysical implications, such as the conductive heat transport in galaxy clusters.

Thesis Supervisor: Professor Mark Vogelsberger
Title: Assistant Professor

Acknowledgments

I would like to thank Dr. Rahul Kannan for his patience, outstanding guidance, and generous support throughout the completion of this thesis.

Contents

Chapter 1

Introduction

In this thesis, we investigate convective instabilities known as the heat-flux-driven buoyancy instability (HBI), and the magnetothermal instability (MTI) in two- and three-dimensional, global hydrodynamic simulations performed by the AREPO code developed by Springel [9], and explore the astrophysical implications of our simulation results. The thesis is structured as follows: in this chapter, we will explain the quenching problem in the galaxy formation theory, which is the physical motivation behind this thesis. This will lead to the discussion of the magnetohydrodynamics (MHD) which describe the dynamics of the plasma in the clusters of galaxies.

In Chapter 2, we will explain the numerical method used in this thesis. In Chapter 3, we describe the numerical setup to our simulations, and present the simulations results

In Chapter 4, we summarize the results and discuss the astrophysical implications.

1.1 Temperature Profile of Galaxy Clusters

Galaxy clusters are the most massive gravitationally bound objects in the universe. Because of their massive structure, surveys of galaxy clusters provide key tests of cosmology. However, the majority of their mass (84%) is in the form of dark matter, with only 3% of their mass in the form of stars. The remaining 13% consists of hot, low-density, magnetized plasma called the intracluster medium (ICM), which

strongly emits X-ray radiation. With the Chandra X-ray Observatory, we are capable of measuring the X-ray luminosity emitted by the ICM to determine its temperature in galaxy clusters as a function of radius. Therefore, by the use of galaxy clusters as a cosmological tool, we are motivated to study the physics of the heating and cooling mechanisms, and the dynamical processes that govern the ICM.

Our understanding of the galaxy formation theory predicts that galaxy clusters with short central cooling times, or cool-core (CC) clusters, should host massive cooling flows, but the large amount of cold gas and stars are not observed [2]. This implies that the radiative losses in cluster cores are balanced by some heating mechanisms, thereby "quenching" star formation in a galaxy.

The quenching of massive galaxies remains a mystery in the galaxy formation theory. Previous studies have invoked the active galactic nucleus (AGN) feedback to be responsible for the temperature profiles. However, the exact details are not known. Others suggest that these temperature profiles might be influenced by a convective instabilities known as the heat-flux-driven buoyancy instability (HBI).

Moreover, X-ray observations of the ICM in cool-core galaxy clusters also suggest that the temperature of the clusters increases with radius at the center, while decreases at the cluster outskirts. This temperature profile makes the gas susceptible to two instabilities known as the heat-flux-driven buoyancy instability (HBI) and the magneto-thermal instability (MTI), which are explained in the next section.

1.2 Magnetohydrodynamics (MHD)

We describe the dynamics of plasma by using the equations of magnetohydrodynamics (MHD). In Cartesian coordinates, the equations for the conservation of mass, momentum, and magnetic flux, and for the evolution of internal energy are

$$\frac{\partial \rho}{\partial t} + \nabla \cdot (\rho \mathbf{v}) = 0, \tag{1.1}$$

$$\frac{\partial}{\partial t}(\rho \mathbf{v}) + \nabla \cdot \left[\rho \mathbf{v} \otimes \mathbf{v} + \left(P + \frac{B^2}{8\pi}\right)\mathbf{I} + \frac{\mathbf{B} \otimes \mathbf{B}}{4\pi}\right] = \rho(\mathbf{g} + \mathbf{f}), \tag{1.2}$$

$$\frac{\partial \mathbf{B}}{\partial t} = \nabla \times (\mathbf{v} \times \mathbf{B}), \quad (1.3)$$

$$\rho T \frac{\mathrm{d}s}{\mathrm{d}t} = -\nabla \cdot \mathbf{j}, \quad (1.4)$$

where ρ is the mass density, $\mathbf{v}$ is the fluid velocity, $\otimes$ is the tensor product, P is the pressure, $\mathbf{B}$ is the magnetid field, $\mathbf{I}$ is the unit matrix, $\mathbf{g}$ is the gravitational field, $\mathbf{f}$ is an externally imposed force, T is the gas temperature, s is the entropy per unit mass and is given by

$$s = \frac{1}{\gamma - 1} \frac{k_B}{m_H} \ln\left(\frac{P}{\rho^\gamma}\right), \quad (1.5)$$

$\mathrm{d}/\mathrm{d}t = \partial/\partial t + \mathbf{v} \cdot \nabla$ is the Lagrangian time derivative, and $\mathbf{j}$ is the directional heat flux.

If the conduction is isotropic, the heat flux $\mathbf{j}$ is opposite to the direction of the temperature gradient

$$\mathbf{j} = -\kappa_{sp}(T) \nabla T, \quad (1.6)$$

where κ_{sp} is the conduction coefficient given by Spitzer [8],

$$\kappa_{sp} = \frac{1.84 \times 10^{-5} T^{5/2}}{\ln C} \text{ ergs s}^{-1} \text{ K}^{-1} \text{ cm}^{-1}, \quad (1.7)$$

where $\ln C \sim 37$ is the Coulomb logarithm.

Since we are interested in the astrophysical application of the dynamics of plasma in galaxy clusters, where the electrons have mean free paths much larger than their gyro-radius, the electrons move along magnetic field lines. Therefore, the thermal conductivity of the plasma becomes anisotropic [4], and the heat flux is modified as

$$\mathbf{j} = -\kappa[\mathbf{b}(\mathbf{b} \cdot \nabla T)], \quad (1.8)$$

where $\mathbf{b} = \mathbf{B}/|\mathbf{B}|$.

We assume the plasma to be an ideal gas with an adiabatic constant $\gamma = 5/3$. So,

we can write the gas temperature in terms of the internal energy per unit mass

$$u = \frac{k_B T}{(\gamma - 1)\mu} = c_v T, \tag{1.9}$$

where μ is the mean molecular weight. We can rewrite Equation (1.8) as

$$\mathbf{j} = -\frac{\kappa}{c_v}[\mathbf{b}(\mathbf{b} \cdot \nabla u)]. \tag{1.10}$$

The final equation for anisotropic thermal conduction then becomes

$$\frac{\partial u}{\partial t} = \frac{1}{c_v \rho} \nabla \cdot [\kappa \mathbf{b}(\mathbf{b} \cdot \nabla) u]. \tag{1.11}$$

The dissipative term in Equation (1.4) implies that fluid displacements in a plasma are not adiabatic. Therefore, the convective and mixing properties of a plasma can be very different from those of an adiabatic fluid. Since we are interested in the ICM, we focus on the "rapid conduction limit," where thermal conduction is much faster than the dynamical time scale of the plasma. In this limit, the convective stability criterion of the plasma is determined by the magnitude of the temperature gradient and the local orientation of the magnetic field, in contrast to the usual Schwarzschild criteria which depends on the entropy gradient [1][7].

1.2.1 Magnetothermal Instability (MTI)

Balbus [1] first considered the case where the gas temperature increases in the direction of gravity, and identified the instability known as the magnetothermal instability (MTI). The basic idea is that when we apply a small, plane-wave perturbation to a plasma in thermal and hydrostatic equilibrium with a weak horizontal magnetic field, the plasma moves along the perturbation and the magnetic field lines follow the fluid displacements. Since the temperature gradient is in the direction of the gravity, upwardly displaced fluid elements are warmer than their surroundings, so they continue to rise and expand. Likewise, the downwardly displaced fluid elements are colder than their surroundings, so they continue to sink. Therefore, a small perturbation

can cause buoyancy instability in this case [1]. The illustration of this instability is shown in Figure 1-1. We will show the simulation results and discuss more about this instability in Chapter 3.

1.2.2 Heat-flux-driven Buoyancy Instability (HBI)

Quataert [7] considered the case where the gas temperature decreases in the direction of gravity, and identified the instability known as the heat-flux-driven buoyancy instability (HBI). In this case, the initial equilibrium state has vertical magnetic field lines and a constant heat flux to ensure that the plasma is in thermal equilibrium. However, the perturbations to the magnetic field lines divert the heat flux, so that the upwardly displaced fluid elements become warmer than their surroundings, while the downwardly displaced fluid elements become colder than their surroundings, hence causing a buoyancy instability as shown in Figure 1-1 by McCourt et al. [4]. We will show our simulation results and discuss more about this instability in Chapter 3.

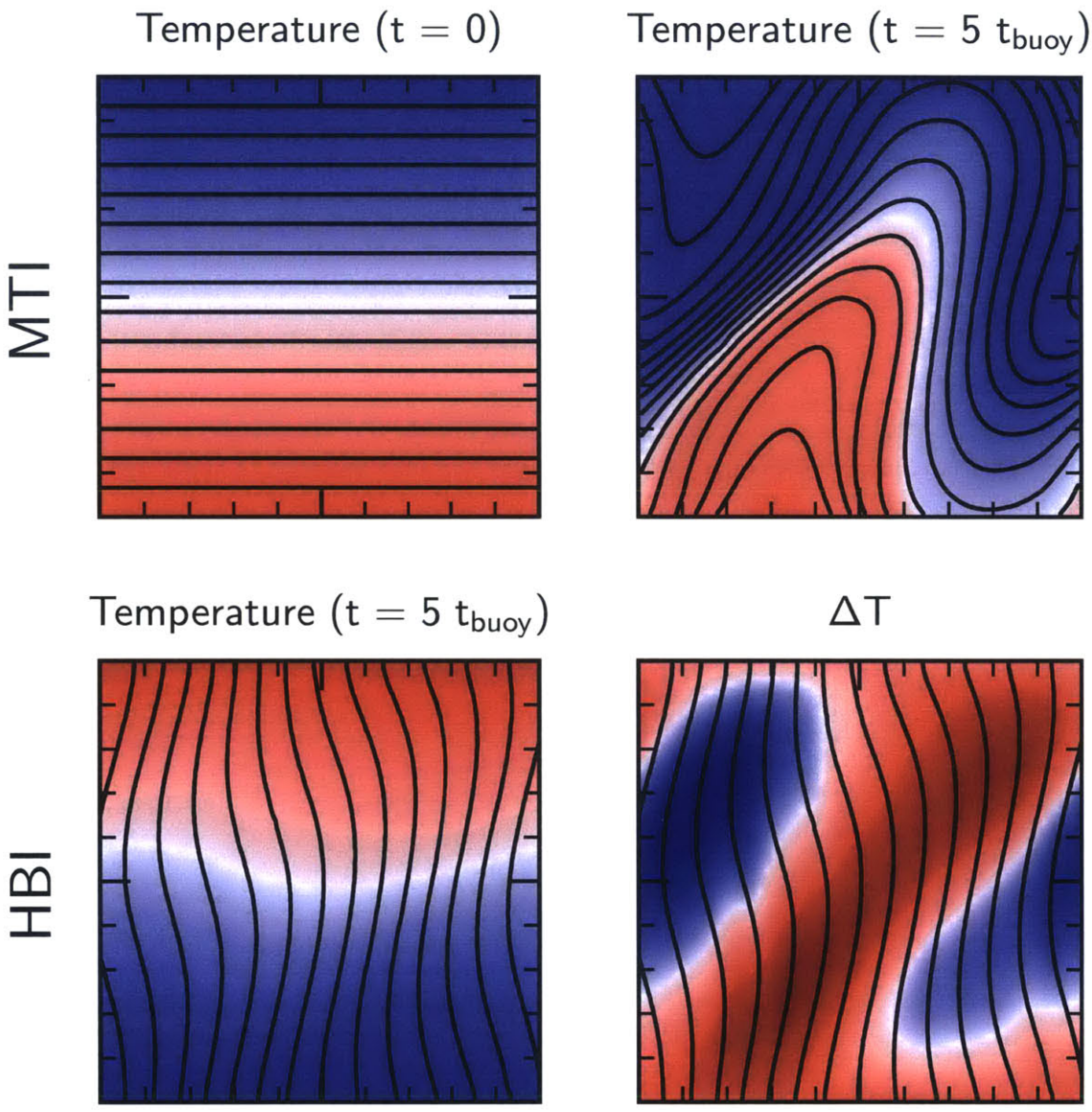

Figure 1-1: Illustration of the linear development of buoyancy instabilities in dilute plasmas from two-dimensional numerical simulations. Color shows the temperature, increasing from blue to red, while black lines trace the magnetic field. This figure is taken from M. McCourt et al.[4].

Chapter 2

Numerical Method

In this chapter, we will explain the basic ideas of the numerical method used in this thesis. Our simulations are performed with the AREPO code developed by Springel [9]. The main reason we use AREPO is that in its Lagrangian mode of operation, the simulation results become Galilean-invariant, meaning that large bulk flows do not introduce large errors, unlike in other ordinary mesh Eulerian codes. The reduced errors in AREPO mean that astrophysical turbulence can be simulated more accurately. This advantage will become clearer when we present the simulation results in the next Chapter. In the chapter, we will first explain the key innovation of the code, the use of a Voronoi tessellation, that allows the mesh to move continuously with the local fluid velocity. Then, we will explain how AREPO simulates thermal conduction and MHD.

2.1 AREPO

The AREPO code uses a finite-volume method to solve the hyperbolic inviscid Euler equations on a moving, unstructured mesh that is able to follow the flow of a fluid. The key method is the use of a Voronoi tessellation to construct the computational mesh by using the positions of a set of mesh-generating points that each defines a computational cell. For a given set of points, a Voronoi tessallation of space consists of non-overlapping cells around each of the mesh-generating points such that each cell contains the region of space closer to it than any of the other points. In 2D, the computational cells are polygons with faces that are equidistant to other mesh-generating points of neighboring cells.

The key advantage of the Voronoi construction is that it allows a continuous deformation of the computational mesh, so the mesh can move in an essentially arbitrary fashion. To illustrate this point, Springel [9] carried out a test of the Kelvin Helmholtz instability shown as a time-sequence in Figure 2-1. The test was initialized as a Cartesian mesh to allow us to visualize the motion of the moving-mesh as a function of time. Each panel gives the density field at times $t = 0.5$, 1.0, 1.5, and 2.0. The Voronoi mesh is also shown in the lower half of each panel. We see that as the Kelvin Helmholtz instability develops, the computational mesh deforms, develops well-defined Kelvin Helmholtz instability billows, and is able to maintain a sharply defined boundary between the two fluids.

The most important result of this construction is that in its Lagrangian mode of operation, the simulation results become Galilean-invariant as shown in Figure 2-2. Springel [9] used the Rayleigh-Taylor instability test to investigate the Galilean invariance of the AREPO code by adding a constant velocity v_x to the initial state. In stratified atmospheres in approximate hydrostatic equilibrium, if a denser fluid lies above a lighter one, energy can be gained if the lighter fluid rises in the gravitational field, hence generating buoyancy-driven fluid motions. As the system is periodic in the x-direction, the evolution of the fluid should not depend on the frame of reference of the observer. Figure 2-2 shows the result of the Rayleigh-Taylor instability calculated

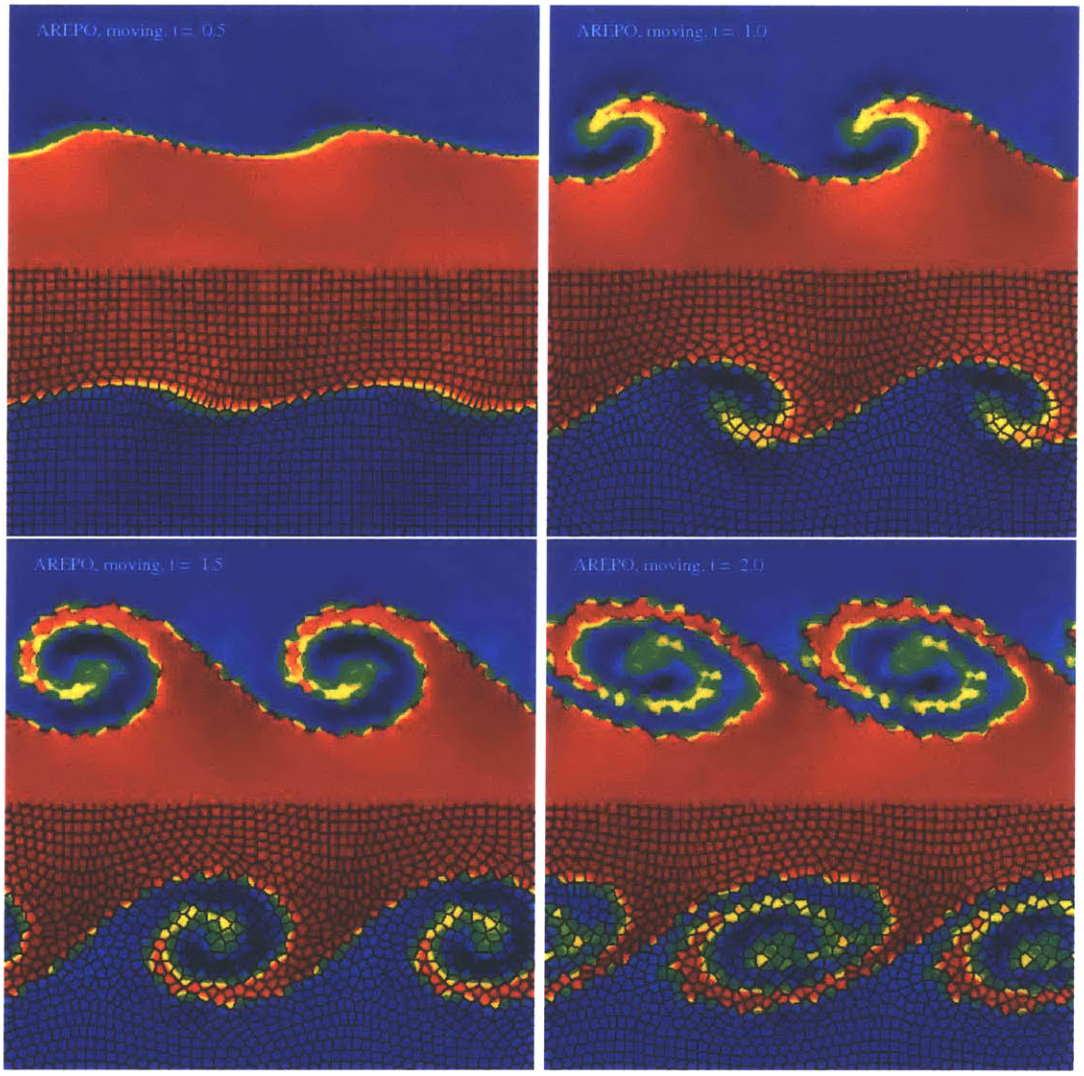

Figure 2-1: These four panels show the time evolution of the Kelvin Helmholtz instability in a low resolution (50×50) test calculation with the moving-mesh method. Each panel gives the density field (at times $t = 0.5$, 1.0, 1.5 and 2.0), with the Voronoi mesh overlaid in black in the lower half of the box. This figure is taken from Springel [9].

with different Galilean boosts v_x in the horizontal direction at time $t = 15.0$. The top row shows the results computed with a moving mesh approach in AREPO, while the bottom row shows the corresponding results from a fixed-mesh calculation with AREPO. Tt is clear that the fixed-mesh Eulerian result is not Galilean-invariant, and depends strongly on the horizontal motion. The horizontal flow velocity leads to a damping of the growth rate of the instability, additional mixing of the fluid, and also to a loss of symmetry. Moreover, for a sufficiently large velocity boost, the instability is suppressed entirely. However, with a moving-mesh method, the results from AREPO become Galilean-invariant. Therefore, astrophysical turbulence can be simulated more accurately by using AREPO.

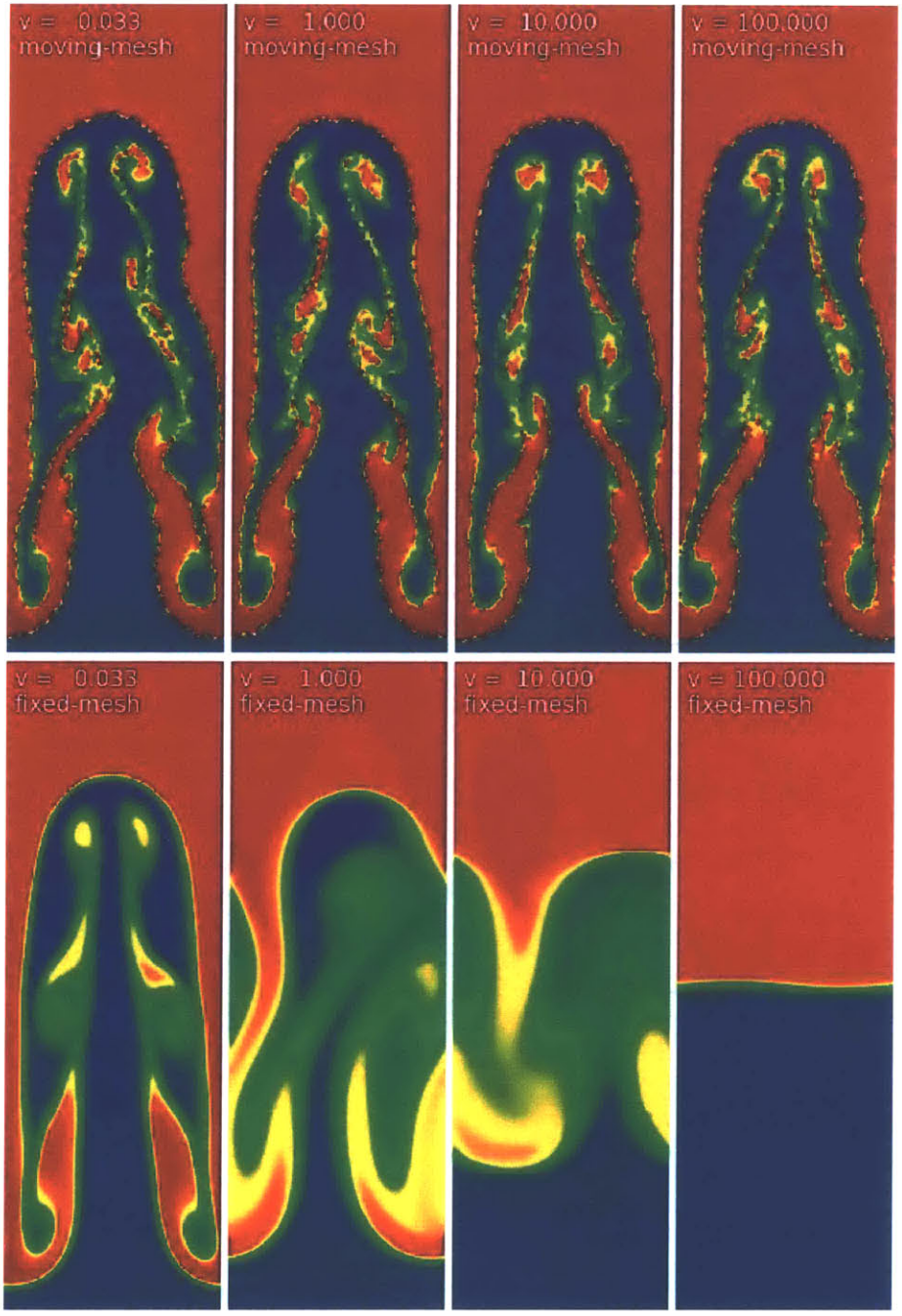

Figure 2-2: Rayleigh-Taylor instability calculated with different Galilean boosts v_x in the horizontal direction (the simulation domain is periodic in the x direction). The correct result should in principal be independent of v (Galilean-invariant). The top row shows the result at time $t = 15.0$ computed with our moving-mesh approach, while the bottom row of panels gives the corresponding results for a fixed-mesh calculation with AREPO. The results from the moving-mesh approach actually produces a Galilean-invariant solution. This figure is taken from Springel [9].

2.2 Anisotropic Conduction and MHD

AREPO uses a stable extremum preserving anisotropic diffusion solver to simulate thermal conduction on a moving Voronoi mesh as presented by Kannan et al. [3]. Widely used discretization method in the numerical modeling of the anisotropic diffusion equation allows heat to flow from lower to higher temperatures, thereby violating the second law of thermodynamics. This unphysical method accentuates temperature extrema, and causes numerical instabilities which can trigger unphysical temperature oscillations.

Our method is to split the one-sided facet heat fluxes into normal and oblique components, by decomposing the gradient of temperature in the coordinate system defined by the cell center and its appropriate neighbors. The neighbors are chosen such that the components of the heat flux in the new coordinate system are all positive. The normal component will always be along the temperature gradient, but the same cannot be said about the other oblique components. So, the oblique flux is non-linearly limited in such a way that the total flux is both locally conservative and also extremum preserving. The extremum preserving property ensures that the second law of thermodynamics is not violated.

The direction of the magnetic fields which decide the direction of heat flow is prescribed by the solution of the ideal magnetohydrodynamics equations described in Pakmor & Springel [5]. The MHD equations are solved through a second-order Runge-Kutta scheme coupled to the approximte HLLD Riemann solver.

Chapter 3

Simulation Results

In this chapter, we present our results from 2D and 3D global simulations of the MTI and HBI from AREPO. The simulation is local in the sense that the computational domain size L is much smaller than the plasma scale height H, while it is global in the sense that $L \geq H$. The local simulation separates the development of the instability from any large-scale response of the plasma, allowing us to study the dynamics of the instability in great detail. The previous work by Kannan et al. [3] performed 2D local simulations of the MTI and HBI. However, the response of the plasma on larger scale can influence the non-linear evolution and saturation of the instabilities, which have astrophysical implication that we will explain in Chapter 4. So, we perform 2D and 3D global simulations of the MTI and HBI by using our implementation of the anisotropic thermal conduction, AREPO, and compare our results to previous simulations performed by McCourt et al. [4].

3.1 Problem Set-up and Integration

Global simulations are defined to be simulations with domain sizes L comparable to, or larger than, a scale-height H. Because of the large domain size, the physical properties of the plasma can vary by an order of magnitude or more across the domain, so the instabilities at different locations can be in a different stages of evolution. For simplicity, we choose initial conditions with a buoyancy time that is constant with

height, meaning that the instabilities at different locations are always in a same stage of evolution. A buoyancy time is defined as $t_{\rm buoy} = \omega_{\rm buoy}^{-1}$ where $\omega_{\rm buoy} = |g\partial \ln T/\partial z|^{1/2}$ is a characteristic frequency for the buoyancy instabilities. We specify

$$g(z) = g_0\, e^{-z/S}, \tag{3.1}$$

Substitute $g(z)$ into the definition of $\omega_{\rm buoy}$ we have

$$u(z) = c_v T(z) = c_v \exp\Big[\pm\frac{S\omega_{\rm buoy}^2}{g_0}(e^{z/S} - 1)\Big], \tag{3.2}$$

where the positive and negative signs represent atmospheres unstable to the HBI and MTI respectively. Since the initial atmosphere is in hydrostatic equilibrium, we solve for $P(z)$, and $\rho(z)$, and get

$$P(z) = \rho(z)(\gamma - 1)u(z), \tag{3.3}$$

$$\rho(z) = \rho_0 \exp\Big[-\int_0^z dz \exp\Big[-\frac{z}{S} \mp \frac{S\omega_{\rm buoy}^2}{g_0}(e^{z/S} - 1)\Big] \mp \frac{S\omega_{\rm buoy}^2}{g_0}(e^{z/S} - 1)\Big], \tag{3.4}$$

where the negative and positive signs represent atmospheres unstable to the HBI and MTI respectively. This integral is numerically solved. The initial conditions are set up as in the global simulations of McCourt et al. [4]. We take $g_0 = 1$ cm s^{-2}, the adiabatic constant, $\gamma = 5/3$, giving $u(z = 0) = 1.5$ erg g^{-1}, $S = 3$ cm, $P(z = 0) = 1$ dyne cm^{-2}, and $\omega_{\rm buoy}^2 = 1/2$. The conductivity in the global simulation is chosen in such a way that the ratio $\kappa_{\rm e}/L$ is the same as it is in the local simulation in McCourt et al.[4], which gives

$$\frac{\kappa_{\rm global}}{L_{\rm global}} = \frac{\kappa_{\rm local}}{L_{\rm local}} = 10\rho\omega_{\rm buoy}L_{\rm local} \tag{3.5}$$

3.2 2D Simulation of the MTI

We perform a 2D global simulation of the MTI. The size of the computational domain is $(1.5\text{ cm})^2$, which corresponds to $L/H = 1/2$. The resolution is 100^2 particles. The initial magnetic field is set to $\mathbf{B} = 10^{-9}\hat{x}$ G. We use the reflective boundary

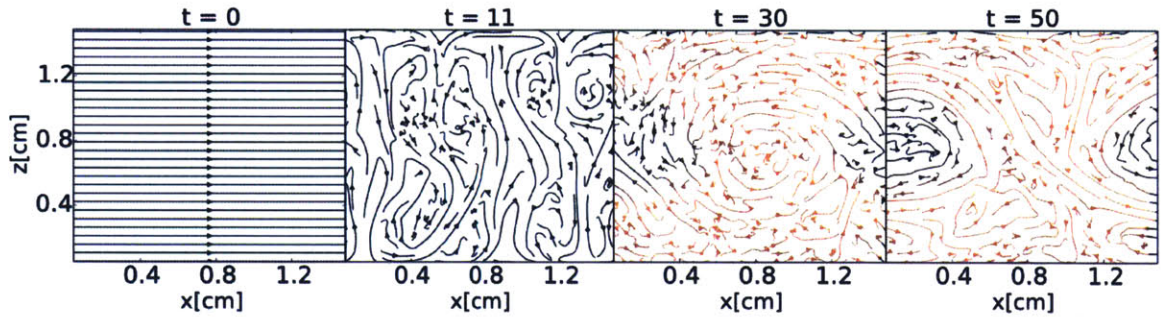

Figure 3-1: Evolution of the magnetic field in the global 2D simulation of the MTI. The system is initially in a horizontal magnetic field. The colors represent the magnetic field intensity at each point, with lighter colors depicting higher magnetic field strengths. The simulation time t is in the units of the buoyancy timescale $t_{\text{buoy}} \sim 1.4$ s.

conditions in the direction parallel to gravity, and the temperature at the upper and lower boundaries are set to be constant. Therefore, the upper and lower boundaries act as sources/sinks of heat during the simulation. We extrapolate the density at the boundary from the cell above and below to enforce hydrostatic equilibrium at the boundary during the simulation. This extrapolation and the reflective boundary condition affect the evolution of the instability. In order to reduce this effect, we insert the anisotropically conducting region between two isotropic buoyantly neutral layers as described in Parrish & Stone [6]. So, the computational domain is divided into three equal regions of length $L/3$ along the direction of gravity. The top and bottom regions have isotropic conduction, while the middle region has fully anisotropic conduction. The setup has a positive entropy gradient, which means that the system is stable in the absence of anisotropic conduction. All the results are for quantities within the anisotropic conduction region. We initialize the simulation in hydrostatic and thermal equilibrium state with horizontal magnetic field lines, and seed this initial condition with a small velocity perturbation of the form

$$v_z = 10^{-4} c_s \sin\Big(\frac{4\pi x}{L}\Big). \tag{3.6}$$

The internal energy, density, and pressure profiles are set according to Equations (3.2)-(3.4).

Figure 3-1 shows the orientation of the magnetic field lines as a function of time. At time $t = 0$, the magnetic fields are initially horizontal. At time $t = 11\ t_{\rm buoy}$, the system becomes unstable, and the magnetic field lines are dragged along the rising and sinking gas. Quataert [7] showed that the maximum growth rate of the MTI goes to zero when $\hat{b_z} = 1$, implying that the MTI should saturate when the magnetic field lines are dragged along the rising and sinking gas, which is when $t = 11\ t_{\rm buoy}$. However, this is not the case. At late times, $t = 50\ t_{\rm buoy} and 100\ t_{\rm buoy}$, the instability continue, and we have sustained turbulence. This is because the displacements in the orthogonal direction to gravity generate a horizontal magnetic field component from the vertical magnetic field. The generated horizontal magnetic field then seeds the instability, and closes the dynamo loop. This process continuously drives the MTI, and sustains turbulence. This is only true because the boundary conditions fix the temperature at the top and bottom of the domain, acting like sources/sinks of heat. If the temperature at the boundary were free to vary, the MTI will saturate by making the plasma isothermal.

Figure 3-2 shows the time evolution of the volume averaged Mach number within the middle region of the simulation where fully anisotropic conduction occurs. The average Mach number is increased to the order of the sound speed due to MIT-driven turbulence. However, we see rapid oscillations of the volume averaged Mach number at early times, implying that the initial condition in our simulations is not stable. Since the simulation is global, and only has a resolution of $(100)^2$ particles, the method that we use to calculate the pressure gradient might not be accurate enough, and gives additional perturbation to the system at early times, resulting in rapid oscillations of the volume averaged velocity. The oscillations will become clearer when we discuss the results from the 3D simulations. However, this behavior at early time does not affect the our results at late times, as we will see that our results agree with previous studies on these instabilities.

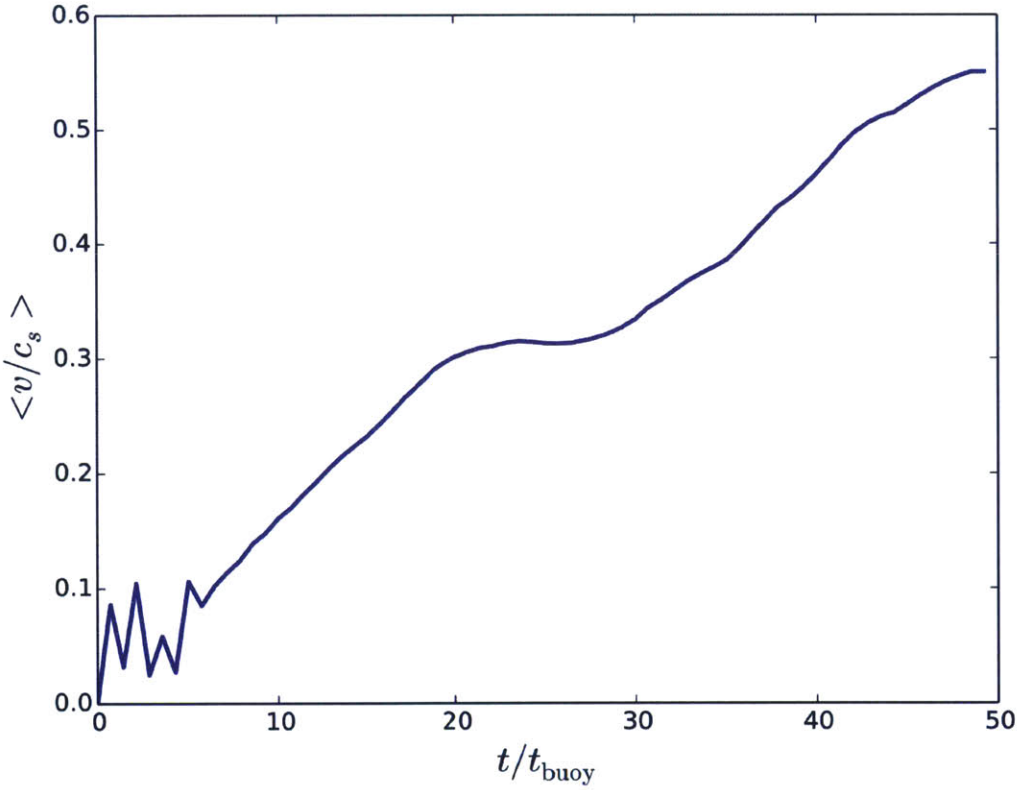

Figure 3-2: Evolution of the volume averaged Mach number of the turbulence generated in the global 2D simulation of the MTI.

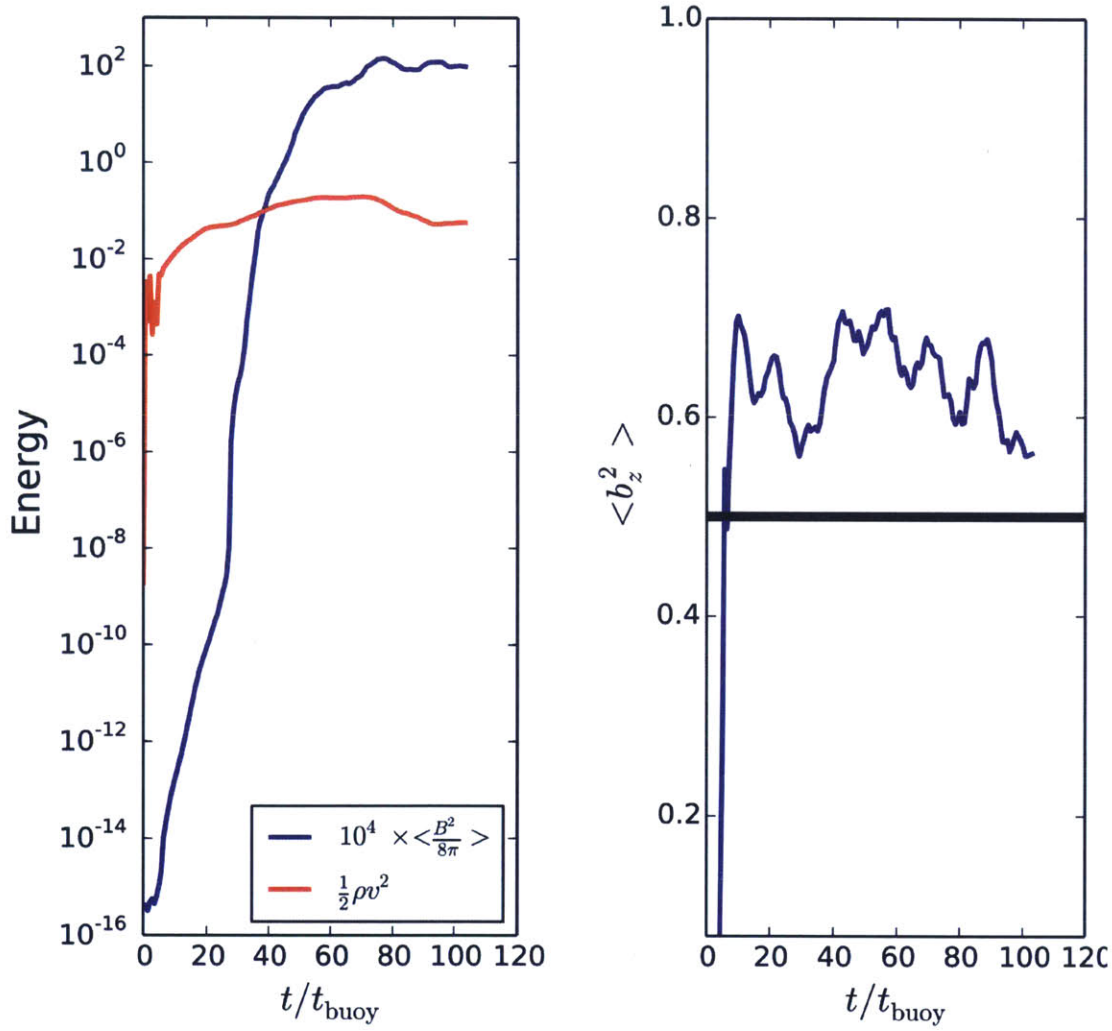

Figure 3-3: *Left panel:* Evolution of the kinetic (red curve) and magnetic (blue curve) energy in the global 2D MTI simulation. *Right panel:* Evolution of the orientation of the magnetic field in the same simulation. The black line indicates the average value of $\hat{b_z}^2 = 0.5$

Figure 3-3 shows the evolution of the kinetic and magnetic energy, and the orientation of the magnetic field in the global 2D MTI simulation. The left panel shows the kinetic energy (red curve) and the magnetic energy (blue curve) as a function of time. The kinetic energy increases rapidly at the beginning, and then slowly saturates, while the magnetic energy is increased exponentially by the turbulence generated by the MTI, and saturates once it reaches equipartition.

The right panel of Figure 3-3 shows the evolution of the orientation of the magnetic field as a function of time. This figure clearly illustrates the non-linear effect of the MTI. During the linear phase of the instability, $t < 10\ t_{\rm buoy}$, the plasma accelerates towards the equilibrium state with $\hat{b_z} = 1$, stretching the magnetic field lines into almost vertical configuration. After the evolution becomes non-linear, the MTI drives sustained turbulence, and the magnetic field evolves asymptotically to the isotropic value.

3.3 3D Simulation of the MTI

We also perform a 3D global simulation of the MTI. The size of the computational domain is $(1.5\ {\rm cm})^3$, which corresponds to $L/H = 1/2$. The resolution is 64^3 particles.

Figure 3-4 shows the evolution of the volume averaged Mach number of the turbulence generated by the MTI in the global 3D simulation. The averaged Mach number reaches 0.1, which is similar to the value obtained by McCourt et al. [4]. However, we also see rapid oscillations of the volume averaged Mach number at early times, implying agaon that the initial condition in our simulations is not stable as we explained in the previous section.

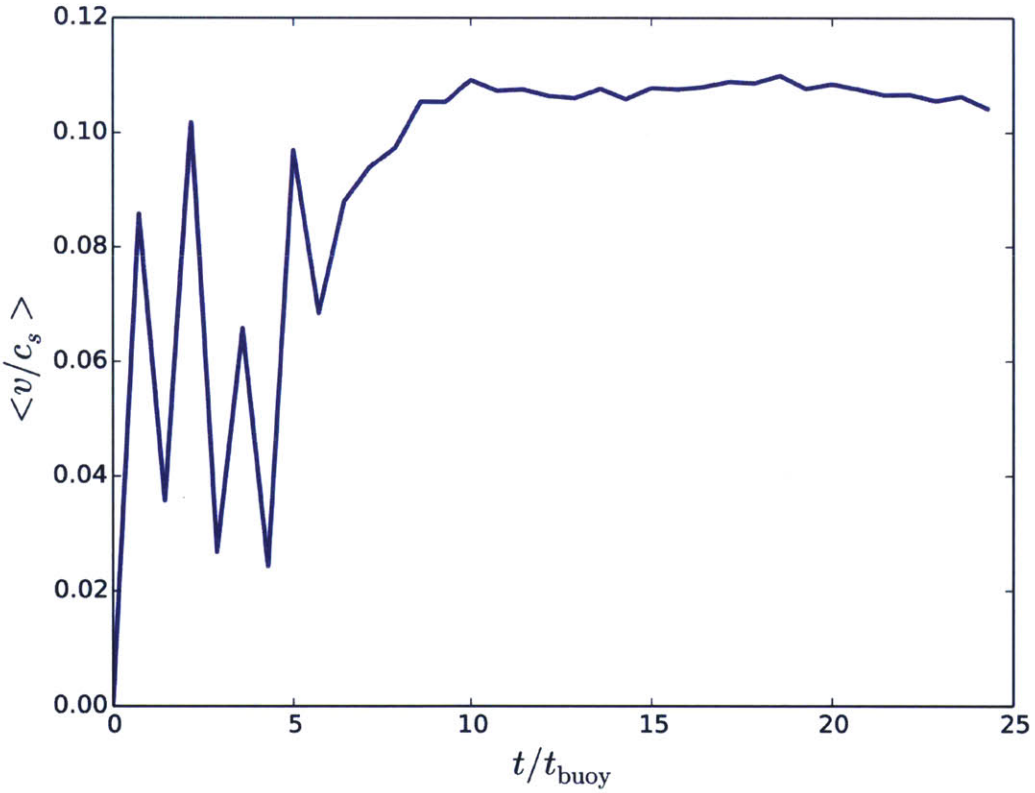

Figure 3-4: Evolution of the volume averaged Mach number of the turbulence generated in the global 3D simulation of the MTI.

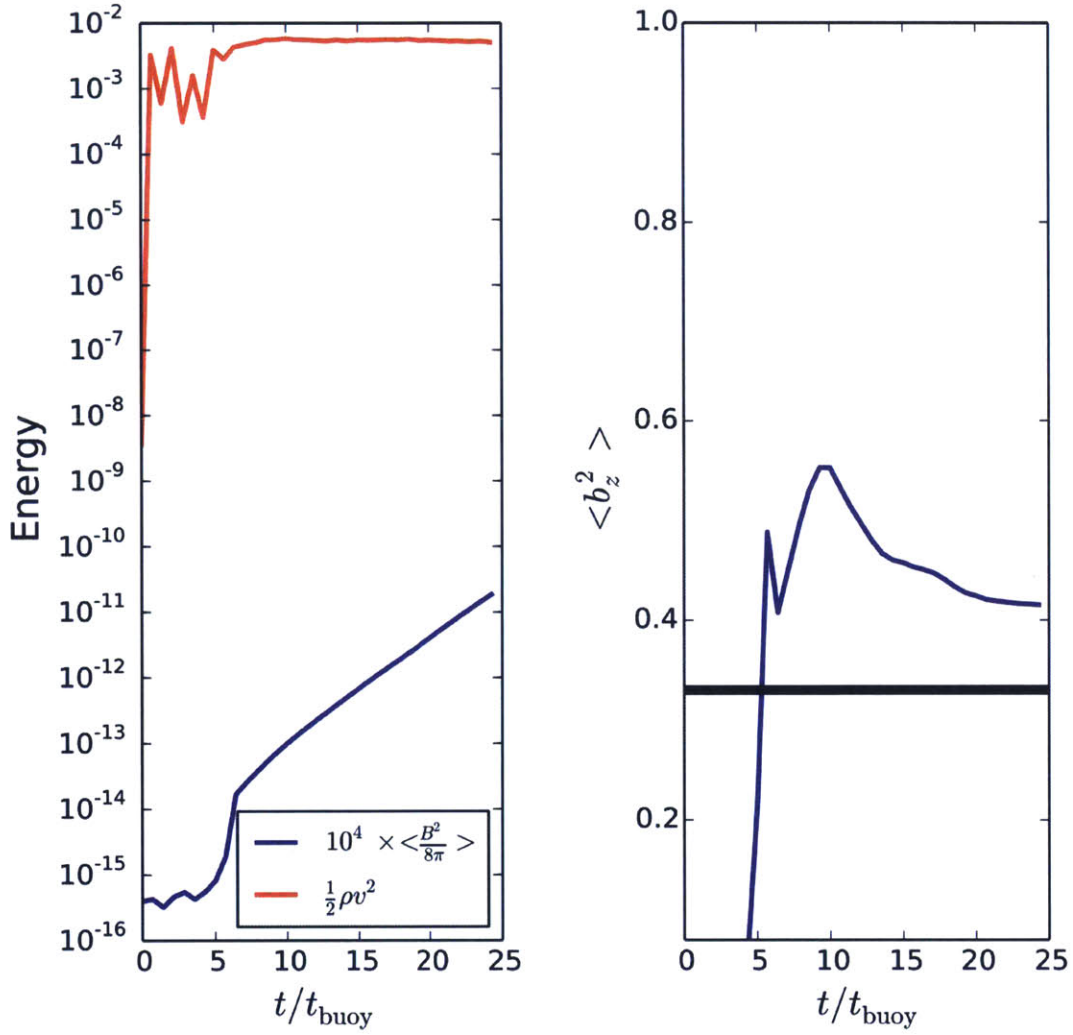

Figure 3-5: *Left panel:* Evolution of the kinetic (red curve) and magnetic (blue curve) energy in the global 3D MTI simulation. *Right panel:* Evolution of the orientation of the magnetic field in the same simulation. The black line indicates the average value of $\hat{b_z}^2 = 0.33$

Figure 3-5 shows the evolution of the kinetic and magnetic energy, and the orientation of the magnetic field in the global 3D MTI simulation. The left panel shows the kinetic energy (red curve) and the magnetic energy (blue curve) as a function of time. The kinetic energy increases rapidly at the beginning, due to the unstable initial condition we explained earlier, and then slowly saturates, while the magnetic energy is increased exponentially by the turbulence generated by the MTI.

The right panel of Figure 3-5 shows the evolution of the orientation of the magnetic field as a function of time. This figure clearly illustrates the non-linear effect of the MTI. During the linear phase of the instability, $t < 5\ t_{\rm buoy}$, the plasma accelerates towards the equilibrium state with $\hat{b_z} = 1$, stretching the magnetic field lines into almost vertical configuration. After the evolution becomes non-linear, the MTI drives sustained turbulence, and the magnetic field evolves asymptotically to the isotropic value of 0.33.

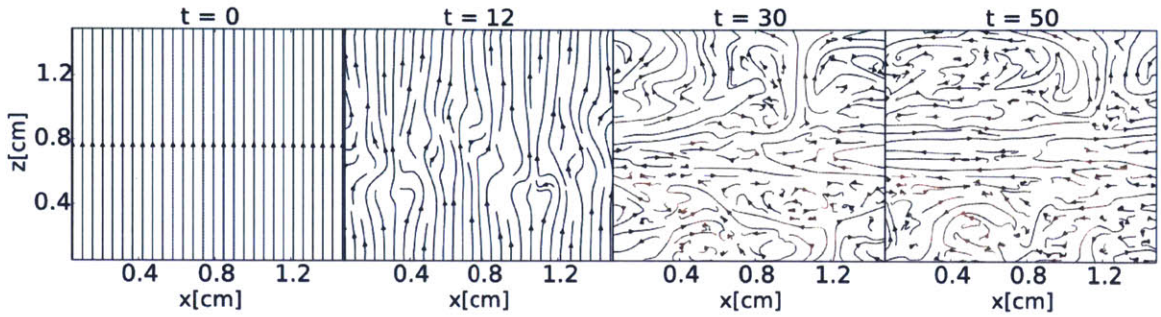

Figure 3-6: Evolution of the magnetic field in the global 2D simulation of the HBI. The system is initially in a horizontal magnetic field. The colors represent the magnetic field intensity at each point, with lighter colors depicting higher magnetic field strengths. The simulation time t is in the units of the buoyancy timescale $t_{\text{buoy}} \sim 1.4$ s.

3.4 2D Simulation of the HBI

We perform a 2D global simulation of the HBI. The size of the computational domain is also $(1.5 \text{ cm})^2$, which corresponds to $L/H = 1/2$. The resolution is 100^2 particles. The initial magnetic field is set to $\mathbf{B} = 10^{-9}\hat{z}$ G. We also use the same boundary conditions as the omes used in the MTI simulations. We initialize the simulation in hydrostatic and thermal equilibrium state with vertical magnetic field lines. Quataert [7] showed that non-zero $\hat{k_x}$ and $\hat{k_z}$, generated converging and diverging magnetic field lines that triggered the HBI. Therefore, we seed this initial condition with a small velocity perturbation of the form

$$v_z = 10^{-4} c_s \Big[\sin\Big(\frac{3\pi z}{L}\Big)\hat{x} + \cos\Big(\frac{4\pi x}{L}\Big)\hat{z}\Big]. \tag{3.7}$$

The internal energy, density, and pressure profiles are set according to Equations (3.2)-(3.4).

Figure 3-6 shows the orientation of the magnetic fields as a function of time. At time $t = 0$, the magnetic fields are initially vertical. By the time $t = 12\ t_{\text{buoy}}$, the magnetic field lines get perturbed enough that the evolution becomes non-linear, and that there are regions where they converge or diverge. These convergence and divergence of the magnetic field lines correspond to regions where the plasma is locally heated or cooled. When the temperature of the fluid decreases in the direction of

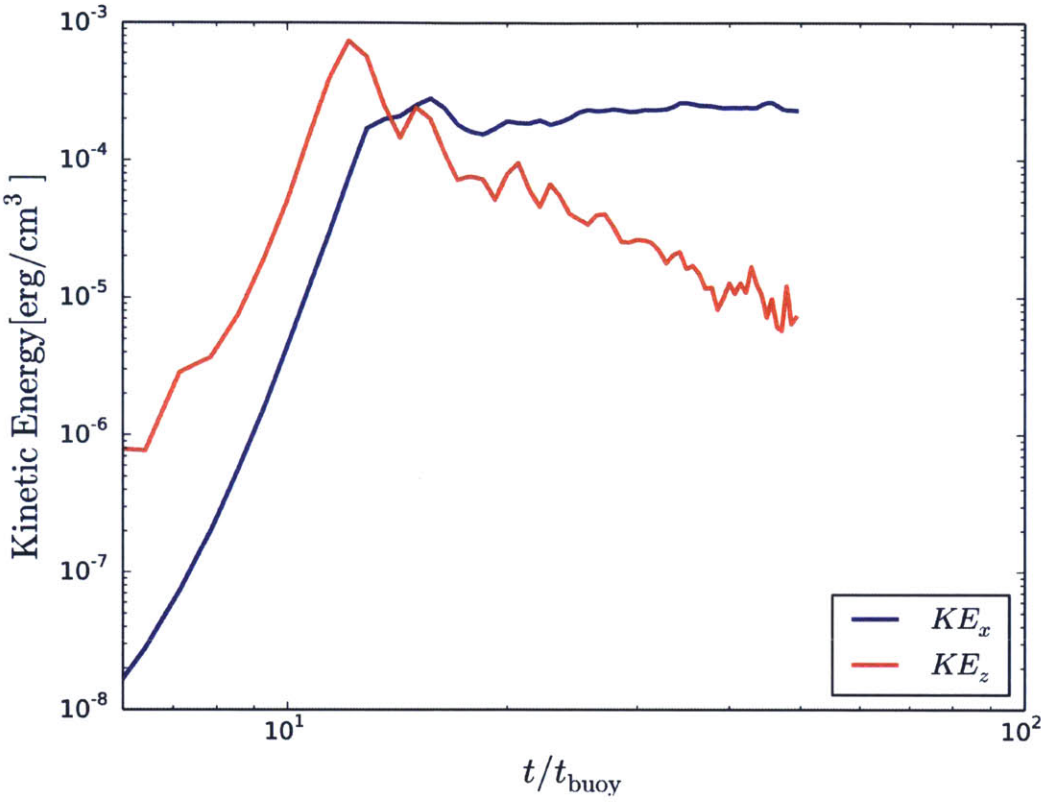

Figure 3-7: Evolution of the vertical (red curve) and horizontal (blue curve) kinetic energy in the global 2D simulation of the HBI.

gravity, a fluid element displaced downward is conductively cooled via the background heat flux, making it colder than the surroundings, and therefor letting it sink further down. On the other hand, a fluid element displaced upward gains energy from the background heat flux, becomes warmer than their surroundings, and buoyantly rises. By the time $t = 50\ t_{\rm buoy}$, the instability saturates and the magnetic field settles into an almost horizontal configuration in the anisotropically conducting region.

Figure 3-7 shows the evolution of the vertical (red curve) and horizontal (blue curve) component of the kinetic energy as a function of time. During the linear growth phase, $t \leq 12\ t_{\rm buoy}$, both components accelerate to equipartition with each other. As the instability saturates, the kinetic energy ceases to grow. The plasma becomes more buoyantly stable, and the kinetic energy in the vertical direction is in the form of stable oscillations, which decay non-linearly, so the vertical component of the kinetic

energy decreases. On the other hand, the horizontal motion is unperturbed, and the horizontal component of the kinetic energy stays at the same value for the entire duration of the simulation.

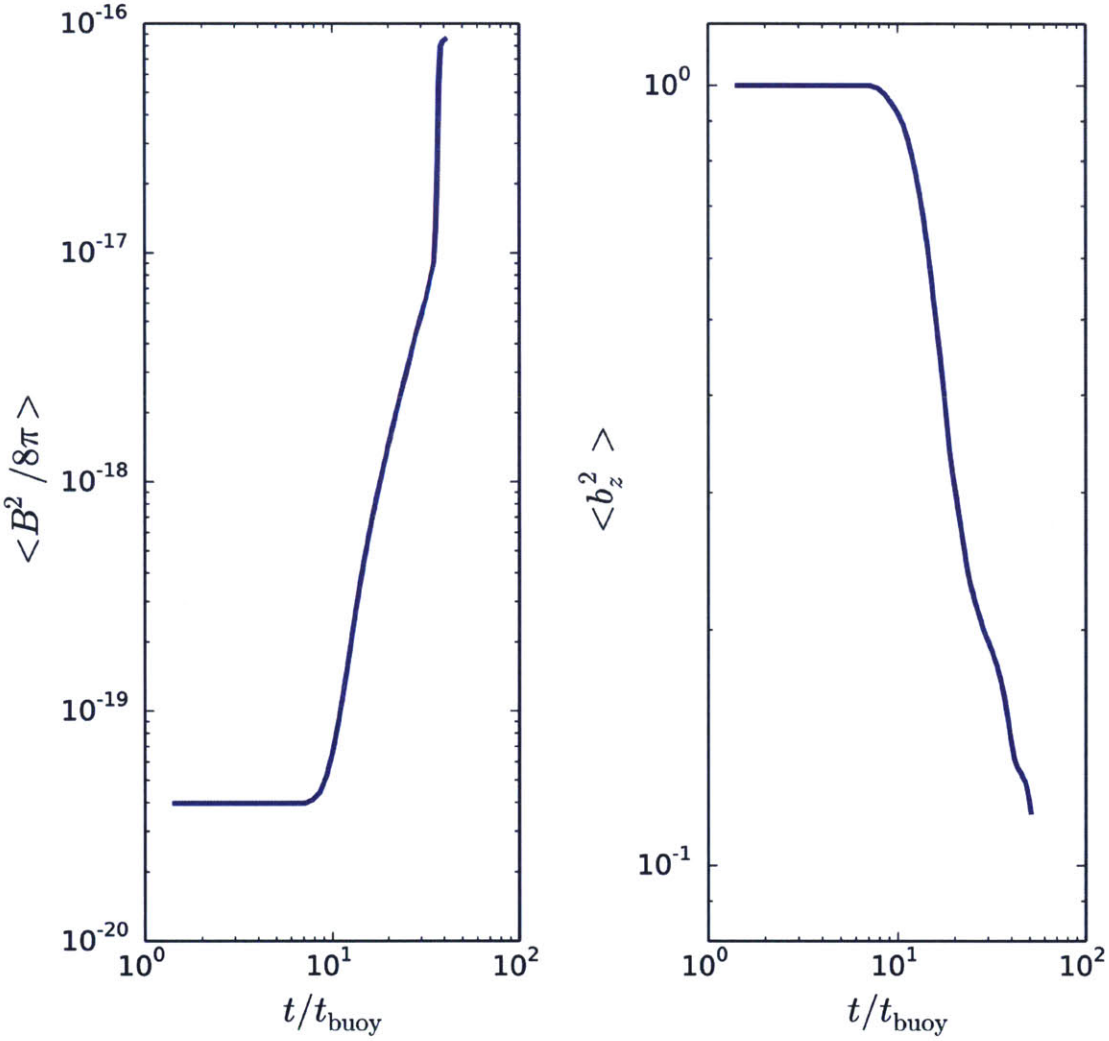

Figure 3-8: *Left panel:* The evolution of the magnetic energy as a function of time in the global 2D simulation of the HBI. *Right panel:* The evolution of the orientation of the magnetic field in the same simulation.

The left panel of Figure 3-8 shows the evolution of the mean magnetic energy as a function of time. The linear exponential growth ends at $t \sim 10\ t_{\rm buoy}$, and most of the evolution of the magnetic field happens afterwards. This evolution is driven by the horizontal motions shown in Figure 3-7, which both amplify and reorient the magnetic field. The field amplification undergoes a brief period of exponential growth, and then roughly grows linearly in time.

The right panel of Figure 3-8 shows the evolution of the orientation of the magnetic field as a function of time. The HBI converts vertical magnetic fields into horizontal ones. The reorienting of the magnetic field also has the effect of severely reducing the conductive heat flux through the plasma. As we see from Figure 3-7, the saturated state of the HBI is buoyantly stable.

3.5 3D Simulation of the HBI

We also perform a 3D global simulation of the HBI. The size of the computational domain is $(1.5\ {\rm cm})^3$, which corresponds to $L/H = 1/2$. The resolution is 64^3 particles.

Figure 3-9 shows the evolution of the vertical (red curve) and horizontal (blue curve) component of the kinetic energy as a function of time. During the linear growth phase, $t \leq 11\ t_{\rm buoy}$, both components accelerate to equipartition with each other. As the instability saturates, the kinetic energy ceases to grow. The plasma becomes more buoyantly stable, and the kinetic energy in the vertical direction is in the form of stable oscillations, which decay non-linearly, so the vertical component of the kinetic energy decreases. On the other hand, the horizontal motion is unperturbed, and the horizontal component of the kinetic energy stays at the same value for the entire duration of the simulation. This result is similar to those of the 2D simulations.

The left panel of Figure 3-10 shows the evolution of the mean magnetic energy as a function of time. The linear exponential growth ends at $t \sim 10\ t_{\rm buoy}$, and most of the evolution of the magnetic field happens afterwards. This evolution is driven by the horizontal motions shown in Figure 3-9, which both amplify and reorient the magnetic field. The field amplification undergoes a brief period of exponential growth,

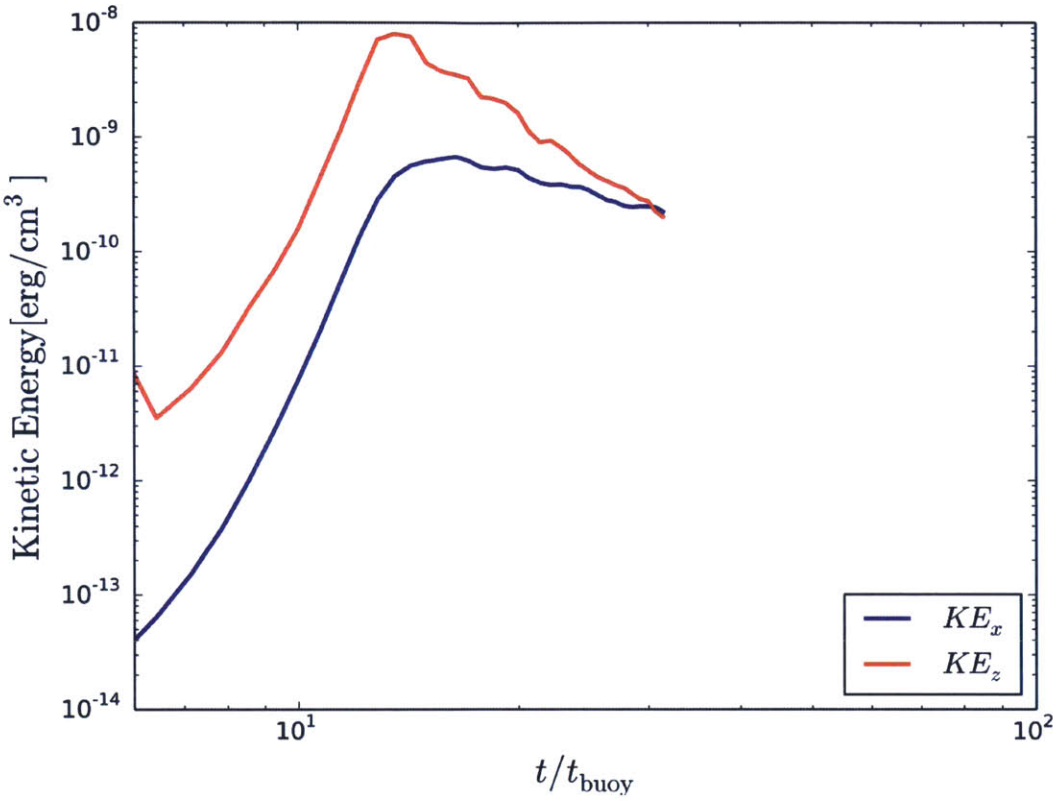

Figure 3-9: Evolution of the vertical (red curve) and horizontal (blue curve) kinetic energy in the global 3D simulation of the HBI.

and then roughly grows linearly in time.

The right panel of Figure 3-10 shows the evolution of the orientation of the magnetic field as a function of time. The HBI converts vertical magnetic fields into horizontal ones. The reorienting of the magnetic field also has the effect of severely reducing the conductive heat flux through the plasma. As we see from Figure 3-7, the saturated state of the HBI is buoyantly stable. The results from 3D simulations are similar to, but are much cleaner than those from 2D simulations. However, we need to continue the 3D simulation for longer period of time to investigate the late time behavior in more detail.

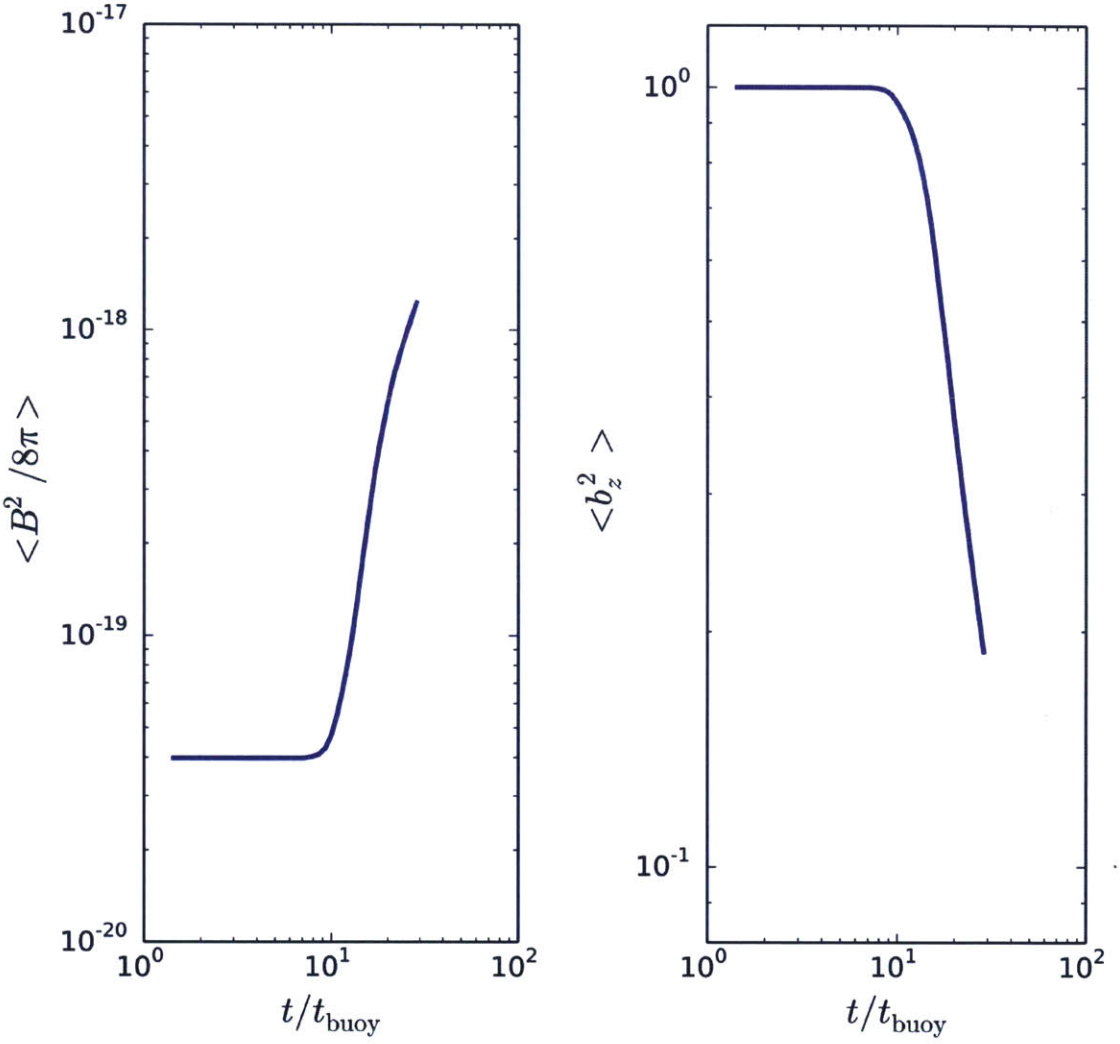

Figure 3-10: *Left panel:* The evolution of the magnetic energy as a function of time in the global 3D simulation of the HBI. *Right panel:* The evolution of the orientation of the magnetic field in the same simulation.

Chapter 4

Conclusions

In this thesis, we have presented the results of the convective instabilities induced by anisotropic conduction in a rapidly conducting plasma. We simulate the magneto-thermal instability (MTI), and the heat-flux-driven buoyancy instability (HBI) in two- and three-dimensional, global hydrodynamic simulations performed by the AREPO code, and verify the results of McCourt et al. [4].

In the MTI simulations, we find that the initially horizontal magnetic fields are quickly disrupted, and the system becomes unstable at early time. The magnetic field lines are dragged along the rising and sinking parcels of gas, reorienting the magnetic field to almost vertical direction. However, the horizontal displacement generates a horizontal magnetic field, and takes the plasma out of its linearly stable state, and re-seeds the instability. The instability grows until non-linear effects dominate, which occurs when $v \sim c_s$. At late times, the orientation of the magnetic field becomes completely random. This turbulence also increases the kinetic and magnetic energy of the gas, so the MTI can generate additional pressure support against gravity. This additional pressure support from the MTI has an important implication on the mass calculation of galaxy clusters, which uses the hydrostatic mass estimation method. This method, however, does not include the effects of anisotropic thermal conduction in the outskirts of galaxy clusters, where the temperature is radially decreasing. This region of clusters is exactly where the MTI can produce significant turbulence. Therefore, a detail study of the effects of the MTI is required for the use of galaxy

clusters for precision cosmology.

In the HBI simulations, we find that kinetic and magnetic energies are amplified to the values that agree with previous works of McCourt et al. [4]. We also find that the HBI, however, saturate quiescently when the magnetic field becomes horizontal. Therefore, the HBI tends to reduce the conductive heat flux. The astrophysical implications of the HBI follow immediately from its saturated state. By reorienting the magnetic field lines, the HBI dramatically reduces the conductive heat flux through the plasma. This implies that the HBI should operate in the innermost region of cool-core galaxy clusters, where the observed temperature increases radially. The HBI then removes thermal conduction as a source of energy for the cores, and potentially worsens the cooling flow problem. In the future work, we plan to investigate the rapid oscillations that occurred at early times in our simulations, and study these conductive instabilities in galaxy clusters.

Bibliography

[1] S. A. Balbus. Stability, Instability, and "Backward" Transport in Stratified Fluids. *ApJ*, 534:420–427, May 2000.

[2] A. C. Fabian. Cooling Flows in Clusters of Galaxies. *Annual Review of Astronomy and Astrophysics*, 32:277–318, 1994.

[3] R. Kannan, V. Springel, R. Pakmor, F. Marinacci, and M. Vogelsberger. Accurately simulating anisotropic thermal conduction on a moving mesh. *MNRAS*, 458:410–424, May 2016.

[4] M. McCourt, I. J. Parrish, P. Sharma, and E. Quataert. Can conduction induce convection? On the non-linear saturation of buoyancy instabilities in dilute plasmas. *MNRAS*, 413:1295–1310, May 2011.

[5] R. Pakmor and V. Springel. Simulations of magnetic fields in isolated disc galaxies. *MNRAS*, 432:176–193, June 2013.

[6] I. J. Parrish and J. M. Stone. Nonlinear Evolution of the Magnetothermal Instability in Two Dimensions. *ApJ*, 633:334–348, November 2005.

[7] E. Quataert. Buoyancy Instabilities in Weakly Magnetized Low-Collisionality Plasmas. *ApJ*, 673:758–762, February 2008.

[8] L. Spitzer. *Physics of Fully Ionized Gases.* 1962.

[9] V. Springel. E pur si muove: Galilean-invariant cosmological hydrodynamical simulations on a moving mesh. *MNRAS*, 401:791–851, January 2010.